A multiscale transport model for Lennard-Jones binary mixtures based on interfacial friction

Ravi Bhadauria and N. R. Aluru[a)]
Department of Mechanical Science and Engineering, Beckman Institute for Advanced Science and Technology, University of Illinois at Urbana-Champaign, Urbana, Illinois 61801, USA

(Received 23 May 2016; accepted 4 August 2016; published online 19 August 2016)

We propose a one-dimensional isothermal hydrodynamic transport model for non-reacting binary mixtures in slit shaped nanochannels. The coupled species momentum equations contain viscous dissipation and interspecies friction term of Maxwell-Stefan form. Species partial viscosity variations in the confinement are modeled using the van der Waals one fluid approximation and the local average density method. Species specific macroscopic friction coefficient based Robin boundary conditions are provided to capture the species wall slip effects. The value of this friction coefficient is computed using a species specific generalized Langevin formulation. Gravity driven flow of methane-hydrogen and methane-argon mixtures confined between graphene slit shaped nanochannels are considered as examples. The proposed model yields good quantitative agreement with the velocity profiles obtained from the non-equilibrium molecular dynamics simulations. The mixtures considered are observed to behave as single species pseudo fluid, with the interfacial friction displaying linear dependence on molar composition of the mixture. The results also indicate that the different species have different slip lengths, which remain unchanged with the channel width. *Published by AIP Publishing.* [http://dx.doi.org/10.1063/1.4961226]

I. INTRODUCTION

The topical problem of mixture transport is of interest in many areas including gas separation,[1] heterogeneous catalysis,[2] flow inside biological membranes,[3–5] and water purification using artificial membranes.[6] A large number of physical systems encountered in transport problems consist of two or more interacting species. Therefore, a deeper understanding of the two component transport problem is of paramount importance. Unlike single component transport problem, which has been studied extensively for simple and complex polar fluids, the theory of mixture transport is a relatively open problem and has been given little attention.

The complexity in modeling the mixture transport problem at nanoscale is twofold. The first challenge is to eliminate the different choice of governing equations. The equations describing the mixture transport in majority of the literature are based on the fluid center of mass (COM) frame of reference.[7] In these methods, the momentum equation has the conventional hydrodynamic stress and strain rate relationship based on the mixture motion. The mixture barycentric (mass averaged) velocity is treated as the advective velocity that enters the species mass balance equations and also appears in the constitutive relationship between the stress and the strain-rate. One can, in principle, decompose the total mass flux of a particular species into advective and diffusive mass fluxes relative to the COM motion and then use Fick's law to close the equation for density.[8,9] Bearman and Kirkwood (BK) have presented the species momentum equation, using expansion around the COM velocity with a statistical-mechanical approach on particle trajectories based on the Liouville and Boltzmann equation framework.[10] The partial stress tensor is identified as the sum of "molecular force" tensor and a diffusion velocity dyadic, where the contribution from the latter term is purely kinetic in nature. The species momentum equations are closed by prescribing the species partial viscosities that relate the species partial stress tensors to the strain-rate tensor of the mixture center of mass velocity. The criticism of this framework is that the partial stress tensor could be non-symmetric even in the absence of angular momentum.[11] Snell *et al.* have tried to readdress this problem by suggesting perturbative expansions around mean species velocities, both from phenomenological macroscopic equations[12] and microscopic statistical basis.[13] The partial viscosity in their work relates the species partial stresses to the species specific strain rates. However, the theory is not very tractable and therefore is not attractive for further investigation. A comprehensive review of these issues is presented elsewhere.[11]

Recently, Kerkhof and Geboers (KG) have critically reviewed the prevalent approaches to mixture transport and have demonstrated the limitations of BK treatment in classical problems like gaseous counter-diffusion and Stefan tube.[14–16] Especially, when the mobilities of the species differ significantly, their individual velocities can be very different from the mixture COM velocity, leading to convergence problems in the BK formulation. To alleviate this, KG have also suggested that the velocity distributions should be centered around average species velocities. Their resulting species momentum balance equation contains species specific stress that is constitutively related to the species individual velocity.

[a)]Electronic mail: aluru@illinois.edu

The second challenge in the theory of mixture transport is to correctly model the effects of confinement and liquid-solid interfacial effects, which are relevant at nanoscale. This entails capturing the inhomogeneity of the relevant parameters along the confined direction, such as density and viscosity variations.[17–20] In addition, fluid-surface interactions along the streaming direction become particularly important to the flow profile, due to the relative motion between the surface and the fluid that is also known as slip. Although significant progress has been made to understand the slip phenomenon for single component fluids from an atomistic point of view,[18,21–23] limited efforts have been undertaken for the mixture transport. Recently, to model this effect, Bhatia and Nicholson have included a continuous friction based term in the governing equation which is active only in the repulsive region of the wall-fluid interaction potential.[19,20] The friction parameter in their model is based on the low density transport diffusion coefficient that can be computed using the oscillator model.[24] The limitation of their model arises from the treatment of the walls, which are diffusive in nature. The incident particle, upon collision with the wall, loses its entire memory of motion in the streaming direction and is re-thermalized, which may not be the case for all surface-fluid interactions in general. This limitation can be addressed by the introduction of Smoluchowski coefficient,[25] which at present can be obtained from experiments or Equilibrium Molecular Dynamics (EMD) computations.[26,27]

Recently, we characterized the slip of a single component fluid using a Generalized Langevin Equation (GLE) based model.[18] The single particle trajectories are evolved using a phenomenological GLE using the total Potential of Mean Force (PMF) as an input. The microscopic thermal noise of the fluid in the confinement is assumed to be equal to that of the unconfined fluid in equilibrium. Making use of the linear response theory,[28] a macroscopic friction coefficient is computed using the wall-fluid structure force autocorrelation and wall-fluid force–velocity cross correlation functions. This friction coefficient can then be incorporated into the one-dimensional (1D) continuum transport model as a Dirichlet boundary condition for the slip velocity. The resulting transport model, by construction, is a multiscale formulation as it embeds the atomic scale details into the continuum model via macroscopic friction coefficient. We also demonstrated that the Dirichlet condition is equivalent to the interfacial friction based Robin type boundary condition (FBC) that describes the force balance between interfacial shear and friction forces.[18]

In this paper, we extend our transport model from a single component fluid to binary Lennard-Jones (LJ) type mixtures. The equations of momentum for the species reflect the shear term dependent on species velocities and an interspecies friction term of the Maxwell-Stefan form.[14–16,19,20] The boundary conditions in the continuum model are applied in the FBC form. The friction coefficient is separately obtained for both species using distinct GLE for each species that evolve single particle trajectories in their respective PMF landscape, thereby retaining the multiscale nature of the formulation. The thermal noise for the species under confinement, characterized by the memory function in the species GLE, is chosen equal to its respective value in the bulk mixture at the same thermodynamic state and molar fraction.

The remainder of the paper is organized as follows: in Sec. II, we present the relevant transport model. We review an empirical potential based quasi-continuum theory (EQT) to calculate the density profiles of the species under confinement in slit channels.[29] Local partial viscosities are obtained as the mass weighted fraction of the local mixture viscosity, where the latter is evaluated using van der Waals one-fluid (vdW1) approximation[30] in conjunction with Local Average Density Method (LADM).[31–33] The slip motion is described by novel species-specific GLE framework that eliminates the need to perform an EMD simulation to compute the relevant correlations. In Sec. III, details of the Molecular Dynamics (MD) and GLE simulations are provided. In Sec. IV, results obtained from the hydrodynamical model are discussed and compared with NEMD simulations. Finally, we draw conclusions in Sec. V.

II. TRANSPORT MODEL

The 1D momentum equation for an arbitrary species α of an isothermal, non-reacting binary mixture can be written as[14–16,19,20]

$$\frac{\mathrm{d}}{\mathrm{d}z}\left[\mu_\alpha^{\mathrm{P}}\frac{\mathrm{d}u_\alpha}{\mathrm{d}z}\right] + m_\alpha\rho_\alpha g_\alpha + \sum_{\substack{\beta=1\\ \beta\neq\alpha}}^{2}\frac{k_{\mathrm{B}}T\rho_\alpha\rho_\beta}{\rho_t D_{\alpha\beta}}\left(u_\beta - u_\alpha\right) = 0, \quad (1)$$

where z is the direction of the confinement, $u_\alpha(z)$ and $u_\beta(z)$ are the unknown streaming direction (x) velocity fields, while $\rho_\alpha(z)$ and $\rho_\beta(z)$ are the concentration fields of the species $\alpha = 1,2$; $\beta = 1,2$ inside the slit channel, $\rho_t(z) = \sum_\alpha \rho_\alpha(z)$ is the mixture density, m_α is the molecular mass, g_α is the applied gravity in the streaming direction of the species α, k_{B} is the Boltzmann constant, and T is the temperature. The partial viscosity $\mu_\alpha^{\mathrm{P}}(z)$ is used to characterize the intraspecies momentum transfer. The variable $D_{\alpha\beta}(z)$ is the binary Maxwell-Stefan diffusivity, the inverse of which is understood as interspecies friction between species α and β. It should be noted that the interspecies friction term in Eq. (1) contains the total contribution of all pairs of α and β species, in a generalized multicomponent case. The binary diffusivities are symmetric, i.e., they follow $D_{\alpha\beta} = D_{\beta\alpha}$, so therefore for a two component system there is only one diffusivity characterizing the interspecies friction. The FBC's are applied at the slip plane located at $z = -L/2 + \delta$, where $\delta = \max(\delta_1, \delta_2)$, and δ_1 and δ_2 denote the nearest distance from the wall where species number densities are greater than a specified tolerance value ρ_{tol}. The FBC can be written as

$$A\mu_\alpha^{\mathrm{P}}(z)\frac{\mathrm{d}u_\alpha(z)}{\mathrm{d}z}\bigg|_{z=-L/2+\delta} = \zeta_\alpha u_{\alpha\mathrm{s}}, \quad (2)$$

where A is the interfacial area and ζ_α is the macroscopic interfacial friction coefficient for species α. The FBC describes the species force balance at the interface, where the wall shear force is balanced by the interfacial friction force that is proportional to the relative velocity between the wall and

the fluid (slip velocity). In addition to the FBC, a second condition that is representative of the symmetry of the velocity profiles at the center point of the slit channel can be written as

$$\left.\frac{\mathrm{d}u_\alpha(z)}{\mathrm{d}z}\right|_{z=0} = 0. \tag{3}$$

Inputs required for this framework are density, viscosity, and the interfacial friction coefficient for both components. The methods to obtain these inputs are discussed below.

A. Inhomogeneous effects: Variation of density and transport properties across confinement

Due to the presence of the confining walls, the density profiles of species show oscillations normal to the wall. Consequently, transport properties such as species partial shear viscosity and binary diffusivities also vary across the confinement. Variations in the densities can be captured using MD and spatial binning or the recently proposed empirical potential based quasi-continuum theory (EQT).[29,34–39] EQT is a multiscale formulation to compute density and the associated PMF profiles along the confinement. Being a continuum based formulation, it is orders of magnitude faster than the particle sampling methods such as MD and Monte Carlo (MC). Coupled with the classical Density Functional Theory (c-DFT) formulation, it can also be used to predict several thermodynamic properties in confined slit systems such as lateral and confined direction pressure, surface tension, solvation force, and adsorption isotherm.[39] EQT has demonstrated significant accuracy over conventional methods such as c-DFT for non-spherical molecules such as carbon-dioxide[36] and SPC/E water[37,38] by incorporating anisotropy in the choice of potentials. The framework is recently extended to binary LJ mixtures, with methane and hydrogen as an example.[29] The framework is robust, tractable and is able to provide density profiles with varying molar fraction of species and temperature with high fidelity.

To capture the viscosity variation along the confined direction, we use the LADM[31–33] on species density profiles to obtain the coarse grained density as

$$\bar{\rho}_\alpha(z) = \frac{6}{\sigma_{\alpha\alpha}^3} \int_{|z-z'|<\sigma_{\alpha\alpha}/2} \left[\left(\frac{\sigma_{\alpha\alpha}}{2}\right)^2 - (z-z')^2\right] \rho_\alpha(z')\,\mathrm{d}z', \tag{4}$$

where $\sigma_{\alpha\alpha}$ is the LJ diameter of species α. The coarse grained density $\bar{\rho}_\alpha$ along with temperature T provides an equivalent thermodynamic state of the species in a locally homogeneous mixture. The potential parameters of a pseudo LJ fluid, which has the same thermodynamic properties (excess potential energy and compressibility) as that of the homogeneous mixture, are computed using the vdW1 approximation[30] as

$$m_\mathrm{f} = \sum_{\alpha=1}^{2} \chi_\alpha m_\alpha, \tag{5a}$$

$$\sigma_\mathrm{f}^3 = \sum_{\alpha=1}^{2}\sum_{\beta=1}^{2} \chi_\alpha \chi_\beta \sigma_{\alpha\beta}^3, \tag{5b}$$

$$\epsilon_\mathrm{f}\sigma_\mathrm{f}^3 = \sum_{\alpha=1}^{2}\sum_{\beta=1}^{2} \chi_\alpha \chi_\beta \epsilon_{\alpha\beta}\sigma_{\alpha\beta}^3, \tag{5c}$$

where $\chi_\alpha = \bar{\rho}_\alpha/\bar{\rho}$ is the molar fraction of species α, $\bar{\rho} = \sum_\alpha \bar{\rho}_\alpha$ being the total homogeneous mixture density; and m_f, σ_f, and ϵ_f are the mass, LJ diameter, and LJ energy parameter of the pseudo LJ fluid. Lorentz-Berthelot (LB) combination rules are used to obtain the cross parameters $\sigma_{\alpha\beta}$ and $\epsilon_{\alpha\beta}$. Once the homogeneous pseudo fluid state of the mixture is characterized, we computed its viscosity to use as mixture viscosity following the correlations provided by Galliéro *et al.*[40] that have strong foundation of the comprehensive dataset provided by Meier *et al.*[41] These correlations are summarized as

$$\mu_\mathrm{f} = \mu_0 + \Delta\mu^*(T^*, \bar{\rho}^*)\,\frac{\sigma_\mathrm{f}^2}{\sqrt{m_\mathrm{f}\epsilon_\mathrm{f}}}, \tag{6a}$$

$$\mu_0 = \frac{5}{16\sigma_\mathrm{f}^2}\sqrt{\frac{m_\mathrm{f}k_\mathrm{B}T}{\pi}}\,\frac{f_\mu}{\Omega^{(2,2)}}, \tag{6b}$$

$$\Delta\mu^* = b_1[e^{b_2\bar{\rho}^*} - 1] + b_3[e^{b_4\bar{\rho}^*} - 1] + \frac{b_5}{(T^*)^2}[e^{b_6\bar{\rho}^*} - 1]. \tag{6c}$$

The dilute gas viscosity μ_0 is at the vanishing density limit, and density dependent residual viscosity $\Delta\mu^*$ is added to get the mixture viscosity μ_f. LADM and vdW1 methods are used to evaluate the reduced homogeneous density $\bar{\rho}^* = \bar{\rho}\sigma_\mathrm{f}^3$ and reduced temperature $T^* = k_\mathrm{B}T/\epsilon_\mathrm{f}$. The collision integral $\Omega^{(2,2)}$ and variable f_μ are discussed in Ref. 42. The coefficients b_γ, where $\gamma = 1,2,\ldots,6$, are provided in Table 1 of Ref. 40. To compute the local partial viscosities μ_α^P, we adopt the approach of Bhatia and Nicholson.[19,20] In their method, the shear stress of the homogeneous mixture is assumed to be equal to the sum of species stresses, yielding the relation $\mu_\alpha^\mathrm{P} = \omega_\alpha\mu_\mathrm{f}$, where ω_α is the mass fraction of species α, and is computed using the species coarse grained density $\bar{\rho}_\alpha$ from Eq. (4). There also exist alternative semiempirical methods to compute partial viscosities of a binary mixture,[16,43] with limited accuracy for mixtures of heavy and light gases.[44]

The LADM serves as an excellent predictive tool to calculate viscosity under certain conditions, and while it uses a coarse grained averaged density, it is still not a non-local model in the strictest sense. A genuinely non-local model takes into account that the viscosity of an inhomogeneous fluid is a non-local kernel in space. Thus, the stress at a point is a convolution of viscosity kernel with the strain rate over the width of the kernel in space. First reported by Todd *et al.*,[45] it is also discussed in recent studies[46,47] where it has been conclusively demonstrated that LADM based methodologies fail when significant velocity gradient reversals are present in the velocity profile.

To compute the interspecies diffusion coefficient D_{12}, we adopt the method proposed by Reis *et al.*[48] Their correlations are generic for LJ chain fluids, so we provide a simplified

expression for monoatomic LJ fluids as

$$D_{12} = \frac{D_0}{\left(\frac{g(\bar{\rho})}{R(\hat{\rho},\,\hat{T})} + \frac{0.04}{\hat{T}^{1.5}}\right)}, \tag{7a}$$

$$D_0 = \frac{3}{8\bar{\rho}\sigma_{12}^2}\left(\frac{k_B T}{2\pi m_{12}}\right), \tag{7b}$$

$$g(\bar{\rho}) = \frac{1}{1-\xi_3} + \frac{3\sigma_{11}\sigma_{22}}{(\sigma_{11}+\sigma_{22})}\frac{\xi_2}{(1-\xi_3)^2} + 2\left[\frac{\sigma_{11}\sigma_{22}}{(\sigma_{11}+\sigma_{22})}\right]^2 \frac{\xi_2^2}{(1-\xi_3)^3}, \tag{7c}$$

$$\xi_l = \frac{\pi}{6}\bar{\rho}\sum_{\alpha=1}^{2}\chi_\alpha \sigma_{\alpha\alpha}^l, \text{ for } l = 2,3, \tag{7d}$$

$$R(\hat{\rho},\,\hat{T}) = \left(1 - \frac{\hat{\rho}}{1.12\hat{T}^{0.2}}\right) \times \left[1 + 0.97\hat{\rho}^{0.5} + 5.1\hat{\rho}^2 + \frac{3.1\hat{\rho} - 2.9\hat{\rho}^{0.5}}{\hat{T}^{1.5}}\right] \times \exp\left(-\frac{\hat{\rho}}{2\hat{T}}\right), \tag{7e}$$

$$\hat{T} = k_B T/\hat{\epsilon},\ \ \hat{\epsilon} = \sum_{\alpha=1}^{2}\sum_{\beta=1}^{2}\chi_\alpha\chi_\beta\epsilon_{\alpha\beta}, \tag{7f}$$

where a reduced mixture density is defined as $\hat{\rho} = \sum_\alpha \bar{\rho}_\alpha \sigma_{\alpha\alpha}^3$, where $\bar{\rho}_\alpha$ is the usual local average density of species α. The reduced mass is defined as $m_{12} = m_1 m_2/(m_1+m_2)$ and is used to calculate the low density kinetic theory limit (D_0) of the interspecies diffusion.[49] Further corrections to the low density estimate of diffusion are incorporated using the hard sphere radial distribution function at the contact $g(\bar{\rho})$[50] and finite density polynomial correction using $R(\hat{\rho},\,\hat{T})$.[51] At this stage, all confinement effects along the confined direction are accounted for. Next we would discuss the streaming direction slip effects.

B. Surface friction: Boundary conditions

In this section, we discuss the method to compute the species-specific friction coefficients ζ_1 and ζ_2. Similar to the single component case, the species interfacial friction is additive.[18,28] Therefore, we first compute the friction coefficient of a single particle j of species α using the expression

$$\zeta_0^j = \frac{\int_0^\infty \langle f_{x,j}^{\rm wf}(0) f_{x,j}^{\rm wf}(t)\rangle {\rm d}t}{k_B T + \int_0^\infty \langle v_{x,j}(0) f_{x,j}^{\rm wf}(t)\rangle {\rm d}t},\ j \in \alpha, \tag{8}$$

where ζ_0^j is the friction coefficient of the particle, $f_{x,j}^{\rm wf}$ and $v_{x,j}$ are the instantaneous streaming direction wall-fluid force and velocity of the particle near the solid wall. The angular brackets $\langle\cdots\rangle$ denote the ensemble average. The time correlation appearing in the numerator is the well known single-particle wall-fluid force autocorrelation function (FACF), while the denominator consists of wall-fluid force–velocity cross-correlation function (FVCCF). The total value of the macroscopic friction coefficient is obtained by adding contributions from all interfacial particles as $\zeta_\alpha = \sum_{j\in\alpha}\zeta_0^j$. This value of the macroscopic friction coefficient is used in the FBC described by Eq. (2), which closes the transport model.

Similar to our previous work,[18] we generate the trajectory of the representative particle j using the GLE. The coarse-grained phenomenological dynamical framework of GLE allows one to evolve the dynamics of the single particle sandwiched between the atomically rough surfaces by taking the streaming and confined direction force fields into account. The dissipative and thermal motion of the particle is accounted by incorporating a non-Markovian friction force and its corresponding random force. The equations of motion can be written as

$$m_\alpha \frac{{\rm d}v_{z,j}(t)}{{\rm d}t} = -m_\alpha \int_0^t K_\alpha(t-t')v_{z,j}(t'){\rm d}t' + f_{z,j}^{\rm tot}(z_j(t)) + R_{z,j}(t), \tag{9a}$$

$$m_\alpha \frac{{\rm d}v_{x,j}(t)}{{\rm d}t} = -m_\alpha \int_0^t K_\alpha(t-t')v_{x,j}(t'){\rm d}t' + f_{x,j}^{\rm tot}(x_j(t), z_j(t)) + R_{x,j}(t), \tag{9b}$$

$$\frac{{\rm d}z_j(t)}{{\rm d}t} = v_{z,j}(t),\ \ \frac{{\rm d}x_j(t)}{{\rm d}t} = v_{x,j}(t), \tag{9c}$$

where m_α is the mass of the particle j representing species α, while $v_{z,j}$ and $v_{x,j}$ are the velocities of the particle in the confined and streaming direction, respectively. The random forces $R_{z,j}(t)$ and $R_{x,j}(t)$ in the corresponding directions have zero mean and are only auto-correlated by virtue of the fluctuation-dissipation theorem as $\langle R_{x,j}(0)R_{z,j}(t)\rangle = m_\alpha k_B T K_\alpha(t)\delta_{xz}$, with δ_{xz} being the Kronecker delta. The corresponding structure based instantaneous force values on particle, i.e., $f_{z,j}^{\rm tot}$ and $f_{x,j}^{\rm tot}$, are sampled using the static mean force maps $F_z^{\rm tot}(z)$ and $F_x^{\rm tot}(x,z)$ that can be analytically calculated as explained in Ref. 18. The presented equations are quite similar to that of the single species case, with one exception being the memory function $K_\alpha(t)$ in Eqs. (9a) and (9b) does not correspond to the pure component. Instead, it describes the noise characteristics of species α for its thermodynamic state in the mixture. The non-Markovian dissipative effects from other species are implicitly accounted in this representation. More explicit representations

of memory function are discussed for colloidal mixtures by Chávez-Rojo and Medina-Noyola,[52] where it is expressed in terms of the partial intermediate scattering functions involving the inter- and intraspecies contributions, but are not attractive due to their complexity and approximate nature.

To calculate the species specific memory function in the mixture, we use the corresponding memory function equation (MFE)[53] that can be written as

$$\frac{\mathrm{d}\psi_j(t)}{\mathrm{d}t} = -\int_0^t K_\alpha(t-t')\psi_j(t')\mathrm{d}t', \tag{10a}$$

$$\psi_j(t) = \frac{\langle \boldsymbol{v}_j(t)\cdot\boldsymbol{v}_j(0)\rangle}{\langle \boldsymbol{v}_j(0)\cdot\boldsymbol{v}_j(0)\rangle}; j\in\alpha, \tag{10b}$$

where $\psi_j(t)$ is the input velocity autocorrelation function (VACF) of species α from a bulk EMD simulation of the corresponding homogeneous mixture. Note that a vector value of particle velocity $\boldsymbol{v}_j(t)$ is used because noise is isotropic in the homogeneous mixture. Also, being a bulk homogeneous case, the FVCCF term does not appear in Eq. (10a). The numerical method to solve Volterra type integro-differential equation (Eq. (10a)) is discussed in Ref. 54. Further discussion on the memory function at different molar compositions of the mixture along with comments on the accuracy of the corresponding confined GLE simulations versus EMD is provided in Sec. IV.

III. SIMULATION DETAILS

Different types of MD simulations are performed in the present work using the LAMMPS package.[55] All molecules are modeled as single site LJ particles, with their interactions described using the LJ 12–6 potential force fields. The majority of the examples in the present work comprise of methane and hydrogen mixtures at variable molar fractions. To test the robustness of the continuum method, additional calculations are performed for methane and argon mixture at a fixed molar fraction. For methane-hydrogen mixtures, an integration time step of 0.5 fs is used, while for methane-argon mixture, a time step of 1 fs is used in MD simulations. The cut-off parameter for all simulations is 1.5 nm, and the interaction parameters are listed in Table I. All cross parameters are obtained using the LB combination rule. All EMD simulations are performed for 12 ns, where the first 2 ns data are discarded to allow system equilibration, and the trajectory data are saved at every 20 fs. We use the convention "X–Y α-β" to identify the bulk state molar composition. For example, a 30–70 methane-hydrogen mixture would mean a binary mixture consisting of 30% methane by molar fraction.

TABLE I. Properties of species considered in present study.

Type	σ (nm)	ϵ/k_B (K)	Mass (g/mol)
Carbon (C)	0.3400	28.0	12.0107
Methane (CH_4)	0.3810	148.1	16.0429
Hydrogen (H_2)	0.2915	38.0	2.0160
Argon (Ar)	0.3410	119.8	39.9480

We first perform a series of EMD simulations of methane-hydrogen mixture in bulk homogeneous environment using a isothermal-isobaric (NPT) ensemble at variable molar fractions. The temperature is set to 300 K using a Nosé–Hoover thermostat[56] with a time constant of 0.2 ps, and the pressure to 1580 bars using a Parrinello-Rahman barostat.[57] The values of chosen temperature and pressure correspond to a supercritical thermodynamic state of the mixture.[29] The total number of particles in each molar composition is kept constant at 1660, only to be redistributed to fix the molar fraction of the species. The volume is allowed to fluctuate to fix the species densities. We perform 5 statistically identical NPT runs for every molar fraction case. The fluctuations in the box volume in these statistically identical NPT runs are averaged to compute the species bulk densities at a given molar fraction. The resulting species and mixture bulk densities for methane-hydrogen cases are plotted in Fig. 1, where it can be seen that the density of the mixture decreases with increasing molar fraction of methane at constant pressure. Further, a NVT run using the averaged box dimensions from NPT calculations is performed for each molar fraction, where the output pressure value is confirmed equal to the target value. These simulations are used for computing and verifying bulk dynamical properties, e.g., VACF to obtain the species memory function $K_\alpha(t)$ using Eq. (10). The procedure is identical for 70–30 methane-argon mixture at 3680 bars and 300 K.

Next, confined EMD runs of the mixture sandwiched between two rigid graphene surfaces (channel width 6.34 nm) are performed keeping the lateral pressure equal to the target pressure. Channel width is defined as the center to center distance between the first layer of wall atoms and is used to calculate the average channel density ρ_{avg}. The other channel widths considered in this work are 3.21 nm, 2.25 nm, and 1.28 nm to test the model accuracy for various length scales and are only simulated for 30–70 methane-hydrogen mixture. For smaller channel widths, the number of species particles

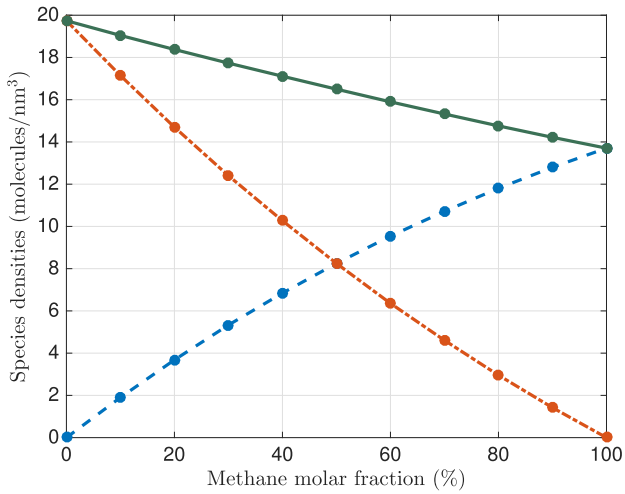

FIG. 1. Mixture (green line, solid) and species bulk density at 1580 bars pressure and 300 K temperature for different molar compositions of a methane-hydrogen mixture. Methane is represented by blue dashed line, while hydrogen is orange dashed-dotted line. Results are averaged over 5 NPT ensembles and errorbars are smaller than the size of the symbols.

is estimated using the linear superposition approximation that ensures the confined fluid pressure is constant under variable channel width.[58,59] The simulation trajectory is divided into 1000 samples of 10 ps, which under ergodic hypothesis serve as ensembles to compute the necessary correlations for friction coefficient.

For confined NEMD simulations, we apply different magnitudes of gravity to test and demonstrate the applicability of the continuum formulation under the linear response regime, where the velocity profile scales linearly with the applied gravity, and the slip length is independent of the applied gravity.[60] The thermostat controlling the temperature is only applied to non-streaming directions to prevent any artifacts in the simulation, i.e., bias in the velocity profiles. To perform the ensemble average, 10 identical simulations are performed, differing only in their initial velocity distribution. Each ensemble is simulated for 30 ns, with the first 10 ns discarded to obtain the fully developed, steady-state velocity profiles.

In the transport model, the slip plane location (δ) is defined to be the larger of the distances δ_1 and δ_2, which correspond to the respective positions where the fluid layers of the two species start to develop. They (δ_1 and δ_2) are estimated using the tolerance on the species densities as 10^{-3} molecules/nm^3. For methane-hydrogen system, this value is approximately 0.24 nm for all molar fraction cases, while for 70–30 methane-argon system, it is 0.3 nm. Its precise location is dependent upon the thermodynamic state and the force-fields used in the MD simulation. To compute the species interfacial friction, 2D GLE simulations are performed with a time step of 0.01 ps, with the production trajectory of 400 ps, with data saved at every other step (0.02 ps). The numerical method for time integration of the GLE is discussed in Ref. 53. First 100 ps of the simulation trajectory was discarded to allow the equilibration of the species GLE particle. Approximately 2×10^4 instances of particle trajectories were generated to compute the relevant time correlations in Eq. (8).

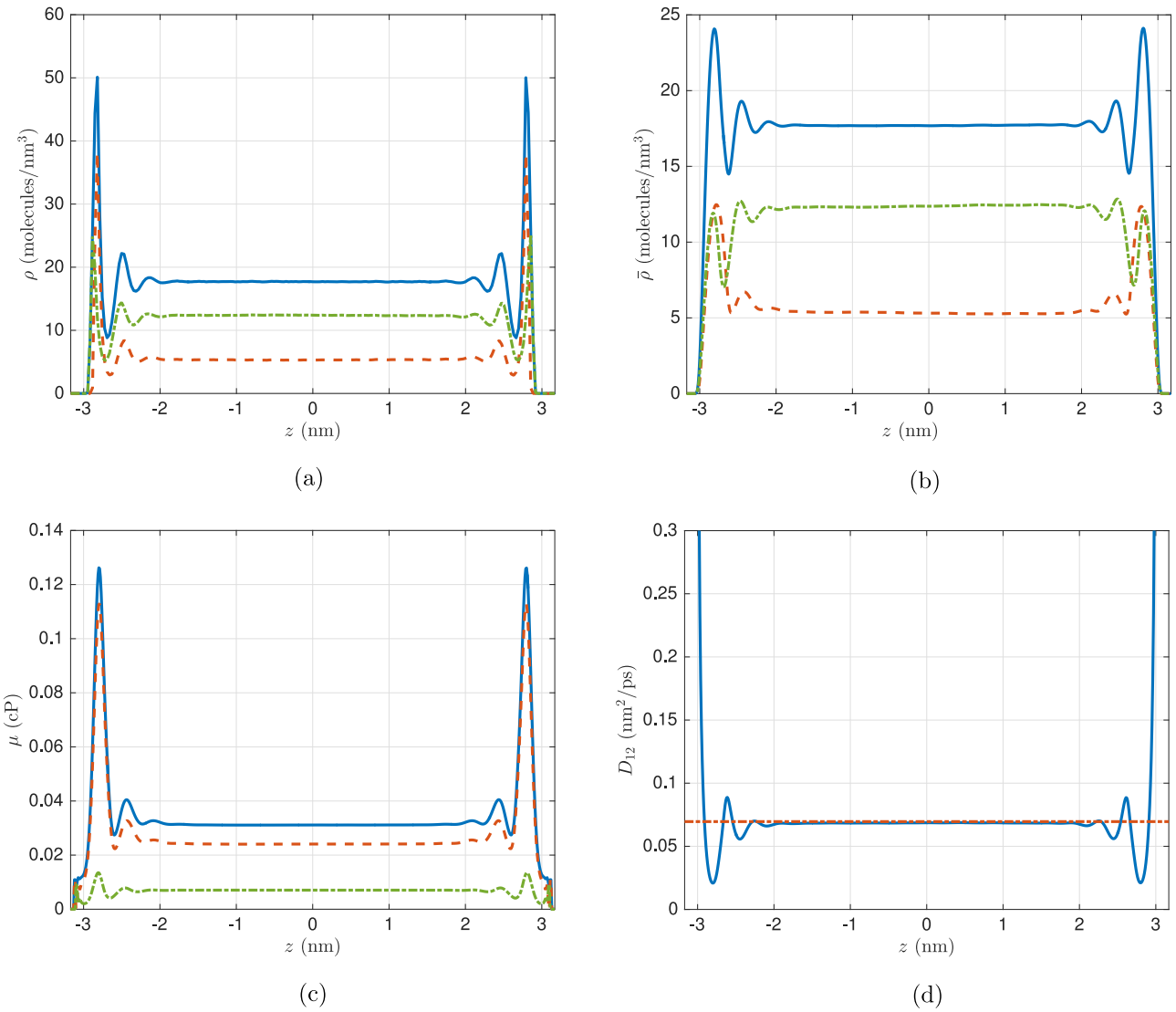

FIG. 2. Variation of (a) local density, (b) local average density, (c) shear viscosity, and (d) interspecies diffusion for 30–70 methane-hydrogen mixture in a 6.34 nm wide graphene slit. Mixture is represented by solid blue line, while methane is orange dashed line and hydrogen is green dashed-dotted line. The dotted red line in (d) is from bulk homogeneous EMD calculations outlined in Ref. 61.

To compare the time estimates, we compared the Central Processing Unit (CPU) time, which is wall-clock time multiplied by the number of parallel processors in a simulation. A single process GLE simulation for 100 ps equilibration and 400 ps production run takes about 120 s in CPU time. In comparison, a typical EMD simulation is orders of magnitude slower (approximately 540 CPU hours to simulate a 12 ns run for the largest system size). Also, GLE can be run on a personal workstation as it uses a single CPU process, and it does not scale with particle number, as compared to EMD/NEMD simulation, which require massive parallelization to curtail the wall-time. The continuum formulation for a binary mixture typically takes 300 s as compared to NEMD, where meaningful data for velocity profiles require 33 230 CPU hours of production runs. Therefore, our GLE/continuum framework provides a massive speedup over NEMD to obtain the velocity profiles.

IV. RESULTS

In this section, we test the accuracy of the continuum framework by comparing the predicted velocity profiles against the ones provided by the NEMD simulations. Using the species density profiles ρ_α, presented in Fig. 2(a) for 30–70 methane-hydrogen mixture in 6.34 nm wide slit channel, we first calculate the local average density $\bar{\rho}_\alpha$ of the species using Eq. (4) and plot them in Fig. 2(b). It can be observed that (a) hydrogen being smaller in size than methane has density peak closer to the wall, and (b) the coarse grained local average density is a homogenized version of local density and contains non-local effects due to the spatial averaging of the latter. The local average density of the mixture is then obtained as the sum of local average density of the species and is used to compute the shear viscosity of mixture as a pseudo LJ fluid using Eqs. (5) and (6) as shown in Fig. 2(c). This is further divided by the local mass fraction $\omega_\alpha(z)$ of the species to obtain the species partial viscosities. Although the number density of the hydrogen is higher than that of methane in the center of the slit channel, the partial viscosity of methane is higher as it is approximately 8 times heavier than hydrogen. We then calculate interspecies diffusion coefficient D_{12} using Eq. (7) and plot it in Fig. 2(d). We also compared the value of D_{12} obtained in the center of the channel with one obtained from the corresponding bulk homogeneous EMD simulation using the method outlined by Heyes in Ref. 61 and found good agreement with the values predicted by empirical correlations.[48]

Next, we compare the effectiveness of the GLE framework to provide species friction coefficient, by comparing the time correlations appearing in Eq. (8) with EMD calculations. As explained previously,[18] we only consider a small interfacial region (about 0.4 nm from the wall) contribution towards the interfacial friction, in conjunction with initial time occupancy based tagging method.[53,62] This is necessary to exclude the viscous effects from the friction computations.[23,28] In order to obtain the memory function, we use the MFE in Eq. (10), with bulk EMD simulation VACF. We plot the resultant memory function of methane (Fig. 3(a)) and hydrogen (Fig. 3(b)) for a homogeneous mixture at 1580 bars and 300 K for different

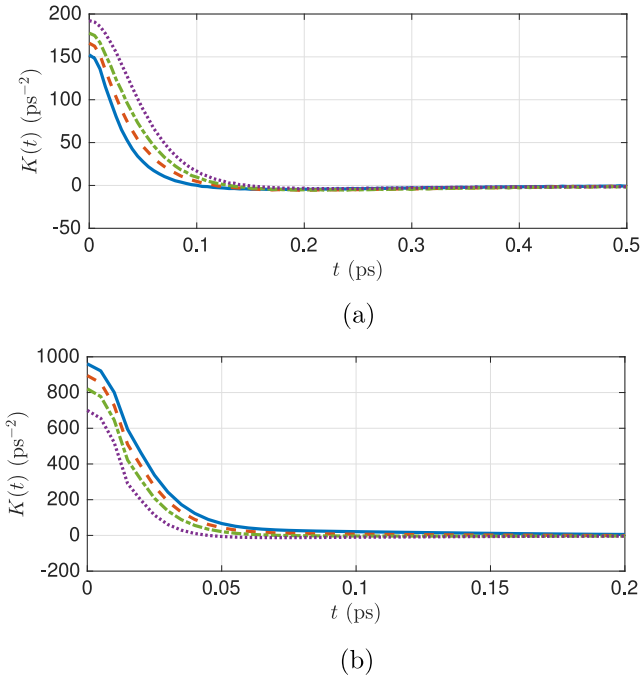

FIG. 3. Memory function at 300 K and 1580 bars of (a) methane in 30–70 (blue line, solid), 50–50 (red line, dashed), 70–30 (green, dashed-dotted), and 100–0 (purple, dotted), and (b) hydrogen in 70–30 (blue line, solid), 50–50 (red line, dashed), 30–70 (green line, dashed-dotted), and 0–100 (purple line, dotted) methane-hydrogen mixture.

molar fractions. As a consistency check, we performed bulk GLE simulations (in the absence of structure based mean forces) of methane and hydrogen to reproduce the input VACF from EMD. It can be understood from the plots that the noise relaxation (memory of dissipation) of hydrogen is faster than that of methane, and change in molar fraction does not alter the noise relaxation time significantly. However, the variance of the thermal force, which is proportional to $K(0)$ as understood by the fluctuation-dissipation theorem, increases with increase in molar fraction of methane, with reversing trends for increase in hydrogen composition. Therefore, one can conclude that methane rich mixtures are more dissipative in nature as compared to hydrogen rich mixtures. We show the comparison of the species FACF calculated from EMD and GLE formulations for 30–70 methane-hydrogen mixture in Figs. 4(a) and 4(b). We observe that there is a good agreement between the two approaches, again validating our choice of using the implicit memory function to compute the transport properties. The contribution of FVCCF to friction coefficient on graphene surface was found to be negligible, in accordance with our previous observations of water on graphene surface.[18]

We now compare the species velocity profiles predicted by the continuum/GLE framework with the ones obtained from NEMD simulations. Figures 5(a) and 5(b) depict the comparison for methane and hydrogen velocities, respectively, for 30–70 methane-hydrogen mixture for different gravity values and channel widths, where a good agreement is observed between the two methods. Similar accuracy is obtained for all molar compositions of the mixture, including the limiting cases comprising of only one species.

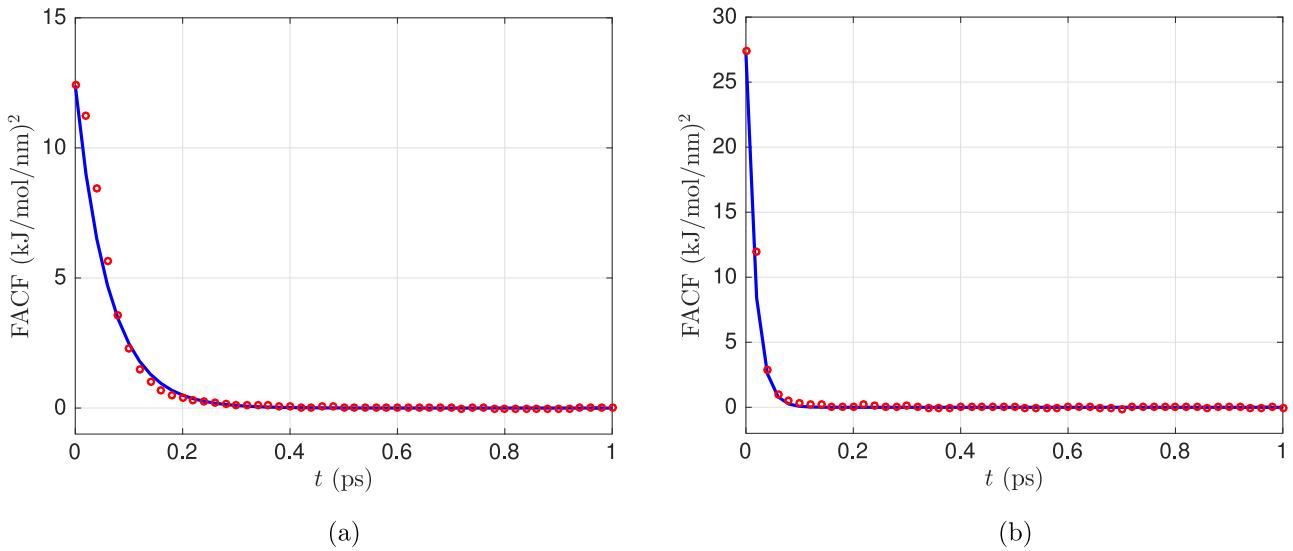

FIG. 4. Wall-fluid FACF from GLE (bold line, blue) and EMD (circles, red) for (a) methane and (b) hydrogen in 30% methane rich mixture composition.

The momentum equation (Eq. (1)) in the limiting case appropriately reduces to that of one component fluid transport because in the limit $\rho_\beta \to 0$, the interspecies friction term vanishes and $\mu_\alpha^{\mathrm{P}} \to \mu_{\mathrm{f}}$. Also, the pseudo fluid viscosity in Eq. (6) obtained from vdW1 approximation (Eq. (5)) reduces to pure component viscosity, thereby providing an internal consistency of this formulation for limiting cases. We also tested the framework for 70–30 methane-argon mixture confined in graphene and observed similar fidelity for velocity profiles as depicted in Figs. 6(a) and 6(b) for methane and argon. By construction, the model includes both viscous and slip effects that are superimposed. The relatively dominant contribution of slip in graphene nanochannels results in plug type of velocity profiles instead of the parabolic type. A systematic analysis of high to low degree of slip with different wall types has been presented before,[17,18] which demonstrate the transition from slip to no-slip type of velocity profiles.

In order to check the accuracy of the framework with differing value of gravity for the two species, we compared the results with $g_1 = 1 \times 10^{-4}$ nm/ps^2 and $g_2 = 2 \times 10^{-4}$ nm/ps^2, for 30–70 methane-hydrogen mixture in a 6.34 nm wide

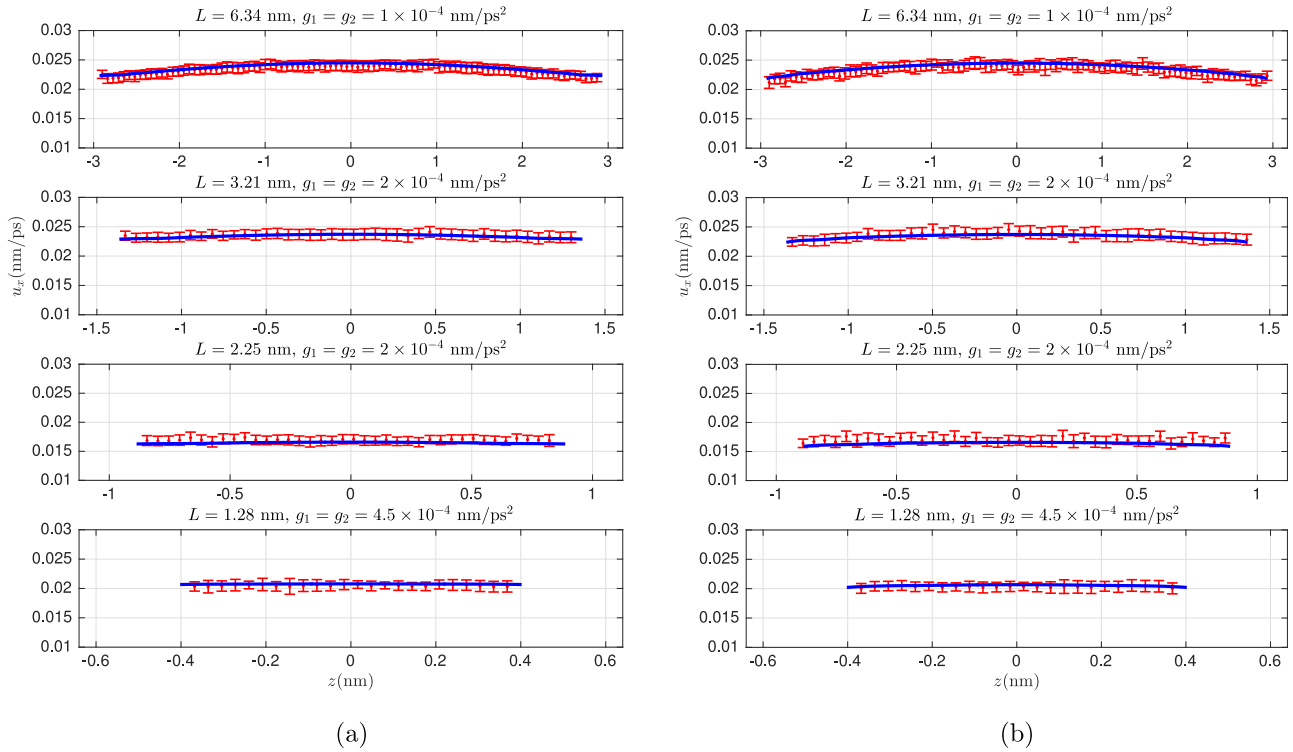

FIG. 5. (a) Methane and (b) hydrogen velocity profiles for 30-70 methane-hydrogen mixture. Continuum results are in solid line (blue), while MD results are represented by error bars (red).

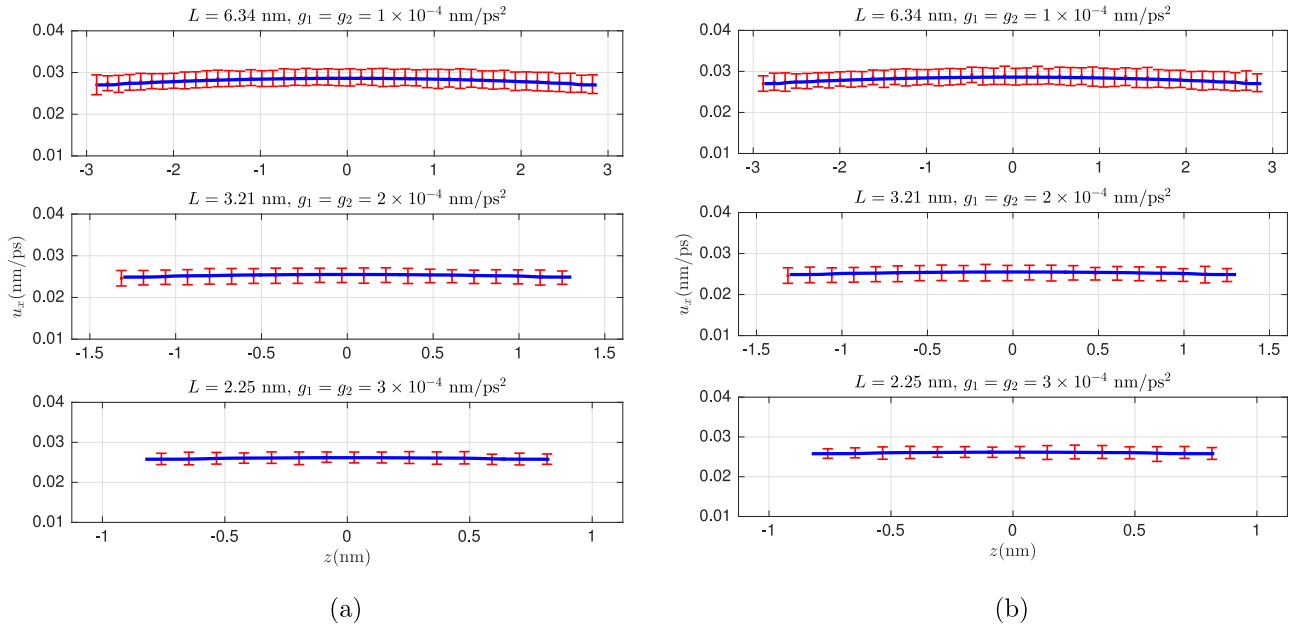

FIG. 6. (a) Methane and (b) argon velocity profiles for 70-30 methane-argon mixture. Continuum results are in solid line (blue), while MD results are represented by error bars (red).

graphene slit as shown in Figs. 7(a) and 7(b). Even under the action of different force per unit mass, the faster species drags the slower species with itself, giving rise to very similar velocity profiles that are corroborated from NEMD and theoretical framework.

Next, we discuss the mixture barycentric velocities. In principle, they can be obtained by taking the mass weighted average of species velocity profiles, but an approximate single fluid representation can also be provided. We start with adding the momentum equation of two species to obtain

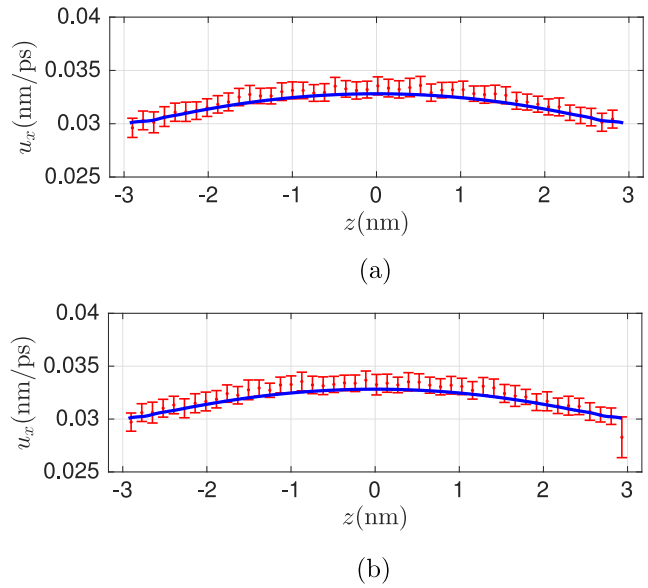

FIG. 7. (a) Methane, and (b) hydrogen velocity profiles of 30-70 methane-hydrogen mixture with methane gravity $g_1 = 1 \times 10^{-4}$ nm/ps^2 and hydrogen gravity $g_2 = 2 \times 10^{-4}$ nm/ps^2. Continuum results are in solid line (blue), while MD results are represented by error bars (red).

$$\frac{\mathrm{d}}{\mathrm{d}z}\left[\mu_1^{\mathrm{P}}\frac{\mathrm{d}u_1}{\mathrm{d}z} + \mu_2^{\mathrm{P}}\frac{\mathrm{d}u_2}{\mathrm{d}z}\right] + m_1\rho_1 g_1 + m_2\rho_2 g_2 = 0, \quad (11)$$

where the last two terms represent the total body force on the mixture, and the term inside the square brackets is the sum of the shear stresses of the species that can be approximated by the mixture shear stress as $\mu_{\mathrm{f}}\,\mathrm{d}u_{\mathrm{f}}/\mathrm{d}z$. Then, the resulting formulation transforms to an equivalent one component transport problem involving pseudo fluid and can be solved with FBC $A\mu_{\mathrm{f}}\,\mathrm{d}u_{\mathrm{f}}/\mathrm{d}z = \zeta_{\mathrm{f}}u_{\mathrm{f}}$ at the slip plane. The effective friction for the mixture ζ_{f} can be apportioned as the sum of species friction as $\zeta_{\mathrm{f}} = \zeta_1 + \zeta_2$, by utilizing its additive nature. As an alternative to the FBC to solve Eq. (11), one can also use the Dirichlet type boundary condition discussed in our previous work for single component transport.[18] We carried out the calculations for the mixture barycentric velocity profile and observed good agreement with the NEMD computed mixture velocity. Next, we computed the value of mixture friction coefficient at different molar concentrations for methane-hydrogen mixture and observed a linear variation as shown in Fig. 8. Therefore, once the pure component friction coefficients of the species are known at a fixed temperature and pressure, the molarity dependent mixture friction coefficient can be predicted by utilizing the linear relationship, without necessitating additional GLE or EMD computations.

Last, we calculate the species slip length $l_{\alpha s}$ using the continuum velocity profiles from the expression

$$l_{\alpha s}\frac{\mathrm{d}u_\alpha(z)}{\mathrm{d}z}\bigg|_{z=-L/2+\delta} = u_{\alpha s} \quad (12)$$

and observed that the species slip length remains unchanged for different channel widths with the same mixture composition (with reference cases being 30–70 methane-hydrogen and 70–30 methane-argon). However, it varies with the mixture composition and is not same for the two species

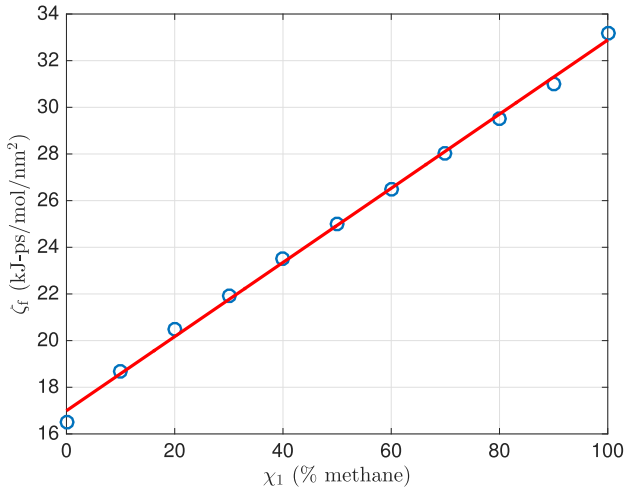

FIG. 8. Friction factor of mixture dependence on methane molar concentration in methane-hydrogen mixtures at 1580 bars and 300 K. GLE computed data points are displayed in blue open circles, while the red line is the linear least squares fit.

TABLE II. Slip lengths (nm) of species on graphene interfaces for selected methane-hydrogen mixtures.

Molar fraction	Methane	Hydrogen
0-100	...	6.6354
30-70	13.8585	3.5225
50-50	12.7025	2.7957
70-30	11.9140	2.0656
100-0	10.5062	...

(see Table II), despite seemingly similar velocity profiles. To understand this, we write the expression for the ratio of the slip lengths

$$\frac{l_{1s}}{l_{2s}} = \frac{\zeta_2}{\zeta_1}\frac{\mu_1^P(z)}{\mu_2^P(z)}\bigg|_{z=-L/2+\delta} = \frac{\zeta_2}{\zeta_1}\frac{\omega_1(z)}{\omega_2(z)}\bigg|_{z=-L/2+\delta}, \quad (13)$$

where we utilize the aforementioned relationship of partial viscosities to pseudo fluid viscosity as $\mu_\alpha^P = \omega_\alpha \mu_f$. It is clear that the equal slip lengths would require the ratio ζ_1/ζ_2 equal to ω_1/ω_2, which is not strictly satisfied.

V. CONCLUSIONS

In this study, we have developed a continuum based hydrodynamic transport model for isothermal, non-reacting mixture transport in slit shaped nanochannels. We have focused on species transport equation instead of mixture motion as a whole. Viscous contributions are incorporated using partial viscosities, which are evaluated using vdW1 and LADM formulation. A Maxwell-Stefan type term is included to characterize the interspecies friction. The boundary conditions are provided in the form of a friction based condition that contains the interfacial friction coefficient. The friction coefficient connects the continuum description of the problem to the atomistics by particle based wall-fluid force autocorrelation and force-velocity cross-correlation functions, which are computed using a refined GLE based dynamical framework for mixtures. The species specific memory function for the GLE is obtained implicitly by utilizing the corresponding MFE of the single particle VACF. The resulting correlations show good agreement with their EMD counterparts. Under application of gravity, the species velocity profiles are predicted that are in excellent agreement with NEMD velocities. The accuracy of the model remains unchanged in cases of species driven by different gravity fields. In the cases considered, the mixture was observed to behave as a pseudo fluid that can be solved with preexisting one component transport models. Furthermore, it is also revealed from the calculations that the effective friction coefficient of the mixture varies linearly with molar composition at constant pressure and temperature and therefore can be directly predicted from the pure component friction coefficients. The slip lengths of the species are observed to be different from each other. The proposed framework is extremely fast and comparable in accuracy with the atomic scale methods used to study the mixture transport problem.

ACKNOWLEDGMENTS

This work was supported by AFOSR (Grant No. FA9550-12-1-0464) and by NSF (Grant Nos. 1264282, 1420882, 1506619, and 1545907). R.B. thanks Tarun Sanghi and Kumar Kunal for helpful discussions on GLE. The authors acknowledge the use of the Taub cluster provided by the Computational Science and Engineering Program at the University of Illinois.

[1]D.-E. Jiang, V. R. Cooper, and S. Dai, Nano Lett. **9**, 4019 (2009).
[2]S. Succi, Phys. Rev. Lett. **89**, 064502 (2002).
[3]E. Tajkhorshid, P. Nollert, M. O. Jensen, L. J. W. Miercke, J. O'Connell, R. M. Stroud, and K. Schulten, Science **296**, 525 (2002).
[4]A. Barati Farimani, N. R. Aluru, and E. Tajkhorshid, Appl. Phys. Lett. **105**, 083702 (2014).
[5]M. S. P. Sansom and P. C. Biggin, Nature **414**, 156 (2001).
[6]M. Heiranian, A. B. Farimani, and N. R. Aluru, Nat. Commun. **6**, 8616 (2015).
[7]R. B. Bird, W. E. Stewart, and E. N. Lightfoot, *Transport Phenomena*, 2nd ed. (John Wiley & Sons, Inc., 2002).
[8]S. R. D. Groot and P. Mazur, *Non-Equilibrium Thermodynamics* (Dover, 1984).
[9]C. Denniston and M. O. Robbins, J. Chem. Phys. **125**, 214102 (2006).
[10]R. J. Bearman and J. G. Kirkwood, J. Chem. Phys. **28**, 136 (1958).
[11]R. Datta and S. A. Vilekar, Chem. Eng. Sci. **65**, 5976 (2010).
[12]F. M. Snell and R. A. Spangler, J. Phys. Chem. **71**, 2503 (1967).
[13]F. M. Snell, R. Aranow, and R. A. Spangler, J. Chem. Phys. **47**, 4959 (1967).
[14]P. J. A. M. Kerkhof and M. A. M. Geboers, Chem. Eng. Sci. **60**, 3129 (2005).
[15]P. J. A. M. Kerkhof and M. A. M. Geboers, AIChE J. **51**, 79 (2005).
[16]P. J. A. M. Kerkhof, M. A. M. Geboers, and K. J. Ptasinski, Chem. Eng. J. **83**, 107 (2001).
[17]R. Bhadauria and N. R. Aluru, J. Chem. Phys. **139**, 074109 (2013).
[18]R. Bhadauria, T. Sanghi, and N. R. Aluru, J. Chem. Phys. **143**, 174702 (2015).
[19]S. K. Bhatia and D. Nicholson, J. Chem. Phys. **129**, 164709 (2008).
[20]S. Bhatia and D. Nicholson, Phys. Rev. Lett. **100**, 11 (2008).
[21]L. Bocquet and J.-L. Barrat, Phys. Rev. E **49**, 3079 (1994).
[22]V. P. Sokhan and N. Quirke, Phys. Rev. E **78**, 015301 (2008).
[23]J. S. Hansen, B. D. Todd, and P. J. Daivis, Phys. Rev. E **84**, 016313 (2011).
[24]O. G. Jepps, S. K. Bhatia, and D. J. Searles, J. Chem. Phys. **120**, 5396 (2004).
[25]G. Arya, H.-C. Chang, and E. J. Maginn, Mol. Simul. **29**, 697 (2003).
[26]V. P. Sokhan, D. Nicholson, and N. Quirke, J. Chem. Phys. **115**, 3878 (2001).
[27]V. P. Sokhan, D. Nicholson, and N. Quirke, J. Chem. Phys. **117**, 8531 (2002).
[28]K. Huang and I. Szlufarska, Phys. Rev. E **89**, 032119 (2014).
[29]M. H. Motevaselian, S. Y. Mashayak, and N. R. Aluru, J. Chem. Phys. **143**, 124106 (2015).

[30]F. J. Blas and I. Fujihara, Mol. Phys. **100**, 2823 (2002).
[31]I. Bitsanis, J. J. Magda, M. Tirrell, and H. T. Davis, J. Chem. Phys. **87**, 1733 (1987).
[32]I. Bitsanis, T. K. Vanderlick, M. Tirrell, and H. T. Davis, J. Chem. Phys. **89**, 3152 (1988).
[33]T. K. Vanderlick, L. E. Scriven, and H. T. Davis, J. Chem. Phys. **90**, 2422 (1989).
[34]A. V. Raghunathan, J. H. Park, and N. R. Aluru, J. Chem. Phys. **127**, 174701 (2007).
[35]T. Sanghi and N. R. Aluru, J. Chem. Phys. **132**, 044703 (2010).
[36]T. Sanghi and N. R. Aluru, J. Chem. Phys. **136**, 024102 (2012).
[37]S. Y. Mashayak and N. R. Aluru, J. Chem. Theory Comput. **8**, 1828 (2012).
[38]S. Y. Mashayak and N. R. Aluru, J. Chem. Phys. **137**, 214707 (2012).
[39]S. Y. Mashayak, M. H. Motevaselian, and N. R. Aluru, J. Chem. Phys. **142**, 244116 (2015).
[40]G. Galliéro, C. Boned, and A. Baylaucq, Ind. Eng. Chem. Res. **44**, 6963 (2005).
[41]K. Meier, A. Laesecke, and S. Kabelac, J. Chem. Phys. **121**, 3671 (2004).
[42]M. M. Papari, Chem. Phys. **288**, 249 (2003).
[43]C. R. Wilke, J. Chem. Phys. **18**, 517 (1950).
[44]R. B. Bird, W. E. Stewart, and E. N. Lightfoot, *Transport Phenomena*, 2nd ed. (John Wiley & Sons, Inc., 2002), p. 27.
[45]B. D. Todd, J. S. Hansen, and P. J. Daivis, Phys. Rev. Lett. **100**, 195901 (2008).
[46]K. S. Glavatskiy, B. A. Dalton, P. J. Daivis, and B. D. Todd, Phys. Rev. E **91**, 062132 (2015).
[47]B. A. Dalton, K. S. Glavatskiy, P. J. Daivis, and B. D. Todd, Phys. Rev. E **92**, 012108 (2015).
[48]R. A. Reis, R. Nobrega, J. V. Oliveira, and F. W. Tavares, Chem. Eng. Sci. **60**, 4581 (2005).
[49]S. Chapman and T. G. Cowling, *The Mathematical Theory of Non-Uniform Gases: An Account of the Kinetic Theory of Viscosity, Thermal Conduction, and Diffusion in Gases* (Cambridge University Press, 1939).
[50]G. A. Mansoori, N. F. Carnahan, K. E. Starling, and T. W. Leland, J. Chem. Phys. **54**, 1523 (1971).
[51]E. Ruckenstein and H. Liu, Ind. Eng. Chem. Res. **36**, 3927 (1997).
[52]M. A. Chávez-Rojo and M. Medina-Noyola, Phys. Rev. E **72**, 031107 (2005).
[53]T. Sanghi and N. R. Aluru, J. Chem. Phys. **141**, 174707 (2014).
[54]B. J. Berne and G. D. Harp, "On the calculation of time correlation functions," in *Advances in Chemical Physics* (John Wiley & Sons, Inc., 2007), pp. 102–106 and 217–222.
[55]S. Plimpton, J. Comput. Phys. **117**, 1 (1995).
[56]S. Nosé, J. Chem. Phys. **81**, 511 (1984).
[57]M. Parrinello and A. Rahman, J. Appl. Phys. **52**, 7182 (1981).
[58]I. K. Snook and W. van Megen, J. Chem. Soc., Faraday Trans. 2 **77**, 181 (1981).
[59]S. K. Das, M. M. Sharma, and R. S. Schechter, J. Phys. Chem. **100**, 7122 (1996).
[60]P. A. Thompson and S. M. Troian, Nature **389**, 360 (1997).
[61]D. M. Heyes, J. Chem. Phys. **96**, 2217 (1992).
[62]E. R. Pinnick, S. Erramilli, and F. Wang, Mol. Phys. **108**, 2027 (2010).